The Duality of Geodesic Voronoi/Delaunay Diagrams For An Intrinsic Discrete Laplace-Beltrami Operator on Simplicial Surfaces

Yong-Jin Liu, Chun-Xu Xu* Ying He† Deok-Soo Kim‡

Abstract

An intrinsic discrete Laplace-Beltrami operator on simplicial surfaces S proposed in [2] was established via an intrinsic Delaunay tessellation on S. Up to now, this intrinsic Delaunay tessellations can only be computed by an edge flipping algorithm without any provable complexity analysis. In the paper, we show that the intrinsic Delaunay triangulation can be obtained from a duality of geodesic Voronoi diagram on S with a proof that this duality exists under two practical assumptions. Then the fast and stable computation of geodesic Voronoi diagrams provides a new way to compute the intrinsic discrete Laplace-Beltrami operator on S. Given the duality, the time and space complexities of the intrinsic Delaunay triangulation are the same as that of geodesic Voronoi diagram, which are $O(m^2 \log m)$ and $O(m)$, respectively, where m is the number of vertices in the intrinsic Delaunay triangulation.

1 Introduction

A simplicial surface S is a simplicial complex in $\mathbb{R}^3$ whose geometric realization is a simplicial 2-manifold mesh. In this paper, we study the simplicial surfaces without boundaries. The discrete Laplace operator on S is defined as the gradient of the discrete Dirichlet energy [4, 14]. Bobenko and Springborn [2] summarized that there are two drawbacks in this definition of discrete Laplace operator: (1) the weights in the discrete Dirichlet energy may be negative and (2) the definition is not intrinsic, that is, two simplicial surfaces which are isometric but have different triangulations may lead to different discrete Laplace operators.

A new intrinsic discrete Laplace-Beltrami operator on simplicial surfaces S was proposed in [2], which overcomes these two drawbacks: (1) its weights are all non-negative and it is called *discrete Laplace-Beltrami operator* due to analogy to the positive weights in classical Laplace-Beltrami operator on a smooth surface with a Riemannian metric [15], and (2) it is *intrinsic*, that is, it is only dependent on an intrinsic Delaunay triangulation of S. Compared to the discrete Laplace operator, the intrinsic discrete Laplace-Beltrami operator has better numerical behavior and finds a wide range of applications in geometric modeling and pattern analysis.

The construction of the intrinsic discrete Laplace-Beltrami operator relies on an intrinsic Delaunay triangulation of a simplicial surface S. Up to now, this intrinsic Delaunay triangulation of S can only be obtained by an edge flipping algorithm [6, 7]. Indermitte et al. [7] showed that this edge flipping algorithm terminates in a finite number of steps and thus the intrinsic Delaunay triangulation exists. The uniqueness of the Delaunay tessellation[1] was proved in [2]. A detailed implementation of the edge flipping algorithm was presented in [6]. Both works [6, 7] did not provide a complexity analysis of the edge flipping algorithm. In [7] a Voronoi diagram was also constructed by using a duality of the intrinsic Delaunay triangulation. However, there is no proof that shows such a duality always exists.

In this paper we present formal definitions for a geodesic Voronoi diagram and an intrinsic Delaunay triangulation in a simplicial surface S. Based on the closed ball property introduced in [5], we prove that if source points of a geodesic Voronoi diagram satisfy two assumptions, the duality between geodesic Voronoi diagram and intrinsic Delaunay triangulation exists. Since the geodesic Voronoi diagram on S can be computed fast and stably [9], the results in this paper suggest a new way to compute the intrinsic discrete Laplace-Beltrami operator using the duality of geodesic Voronoi diagram on S. Based on the duality and the known time and space complexities of geodesic Voronoi diagram [11], the time and space complexities of the intrinsic Delaunay triangulation on S is obtained.

2 Preliminaries

A geometric realization of a simplicial surface in $\mathbb{R}^3$ is a simplicial 2-manifold mesh $\mathcal{M}$, which is flat except at isolated points, called *cone points*, where each point has a cone neighborhood. Denote by V, E and T the set of vertices (i.e., cone points), edges and triangular faces in

*TNList, Department of Computer Science, Tsinghua University, Beijing, China, liuyongjin@tsinghua.edu.cn

†School of Computer Engineering, Nanyang Technological University, Singapore, yhe@ntu.edu.sg

‡Department of Mechanical Engineering, Hanyang University, Seoul, Korea, dskim@hanyang.ac.kr

[1] A Delaunay triangulation is obtained from the Delauany tessellation by triangulating the non-triangular faces.

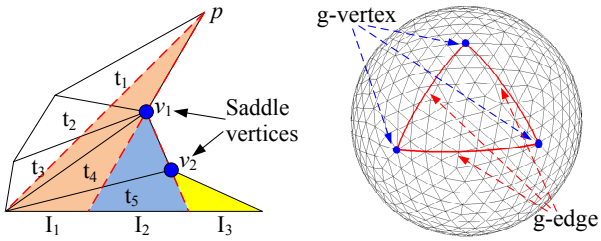

(a) Geodesic paths (b) Geodesic triangle

Figure 1: Geodesic path and triangle. (a) Geodesic paths between points p and q inside triangles $(t_1, t_2, t_3, t_4, t_5)$, which are unfolded into a plane. For the source point p, if the target point $q \in I_1$, the geodesic path is a line $\overline{pq}$; if $q \in I_2$ (or $q \in I_3$), the geodesic path is a polyline $\overline{pv_1q}$ (or $\overline{pv_1v_2q}$). (b) A geodesic triangle in a spherical mesh. Three boundary g-edges are shown in red and g-vertices are shown in blue dots.

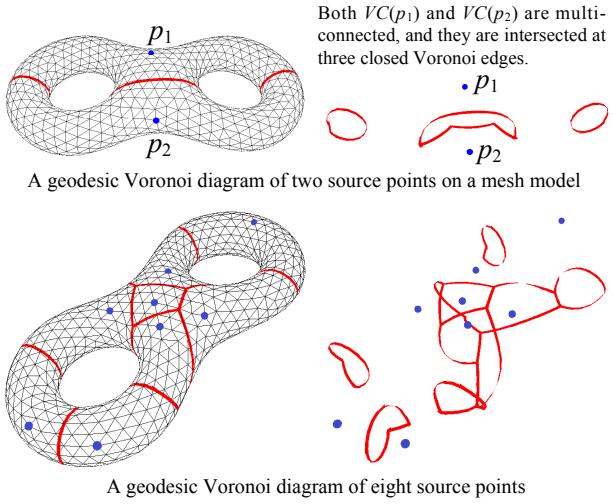

Figure 2: Two geodesic Voronoi diagrams of a set of source points (shown in blue) in an eight model: the trimmed bisectors (i.e., Voronoi edges shown in red) partition the surface into regions and each region is a Voronoi cell of a source point. The Voronoi diagram is shown with (left) and without (right) surface rendering. Note that some Voronoi cells intersects at more than one Voronoi edge and some Voronoi cells are multi-connected (i.e., they are not simple regions). So this general Voronoi diagram does not have a dual intrinsic Delaunay triangulation as defined in Section 2.

$\mathcal{M}$. In this paper, we make the mesh vertices and cone points interchangeable.

The shortest path between any two points p and q in $\mathcal{M}$ is a geodesic and its geodesic distance is denoted by $d_g(p, q)$. In $\mathcal{M}$, a geodesic is a polyline going through a set of edges and cone points. A geodesic structure was analyzed in [12], which use the fact that when the triangles passed by these edges are unfolded into a plane, the geodesic become a straight line segment. In V, denote by saddle vertices those vertices in $\mathcal{M}$ whose total surrounding angle is larger than or equal to 2π. It was proved in [12] that if a geodesic passes through some mesh vertices other than its two endpoints, these mesh vertices must be saddle vertices (Figure 1(a)).

A geodesic triangle t^g in $\mathcal{M}$ is a simple region (i.e., it is homeomorphic to a planar disk and its boundary is a simple, closed curve) whose boundary consists of three geodesics (Figure 1(b)). Each geodesic in the boundary ∂t^g of t^g is called a *g-edge* of t^g and each endpoint of a g-edge in ∂t^g is called a *g-vertex* of t^g. A geodesic triangulation in $\mathcal{M}$ is a family T^g of geodesic triangles t_i^g, such that

- $\bigcup_{i=1} t_i^g = \mathcal{M}$,
- If $t_i^g \cap t_j^g \neq \emptyset$, $i \neq j$, then $t_i^g \cap t_j^g$ is either a common g-edge or g-vertex of t_i^g and t_j^g.

Every smooth 2-manifold admits a triangulation [1]. A geodesic triangulation in $\mathcal{M}$, however, need to be carefully constructed. For example, between two points in a 2-manifold, there may not be a unique geodesic between them, such as the north and south poles of a sphere model.

In $\mathcal{M}$, an open geodesic disk centered at a point $p \in \mathcal{M}$ of radius r is defined as $D_r^g(p) = \{q \in \mathcal{M} : d_g(p, g) < r\}$. The boundary of $D_r^g(p)$ is $\partial D_r^g(p) = \overline{D}_r^g(p) \setminus D_r^g(p)$, where $\overline{D}_r^g(p)$ is the closure of $D_r^g(p)$. A regular region Ω in $\mathcal{M}$ is called an embedded disk if Ω is homeomorphic to a planar disk. A geodesic disk that is also an embedded disk is denoted as an *e-g-disk*. A geodesic triangulation T^g is a Delaunay geodesic triangulation if and only if $\forall t^g \in T^g$, there is an e-g-disk D such that ∂D passes through three g-vertices of t^g and D does not contain any g-vertex of T^g.

Given a set of points $P = \{p_1, p_2, \cdots, p_m\}$ in $\mathcal{M}$, the Voronoi cell of p_i in $\mathcal{M}$ is defined in [9] by $\mathcal{VC}(p_i) = \{q : d_g(p_i, q) \leq d_g(p_j, q), i \neq j, q \in \mathcal{M}\}$ (Figure 2). The geodesic Voronoi diagram of P, $\mathcal{GVD}(P) = \{\mathcal{VC}(p_1), \mathcal{VC}(p_2), \cdots, \mathcal{VC}(p_m)\}$, forms a tessellation of $\mathcal{M}$, since all Voronoi cells are mutually exclusive or semi-exclusive, $\bigcup_{i=1}^{m} \mathcal{VC}(p_i) = \mathcal{M}$.

In the Euclidean plane, we can construct the dual graph of the Voronoi diagram of point set P by connecting by line segments all pairs of points from P whose Voronoi cells share a common Voroni edge [13]. When the set P is in a general position (i.e., no four points on a circle or three points collinear), the dual can be shown to be the planar Delaunay triangulation. In a 2-manifold $\mathcal{M}$ there may be no duality between geodesic Voronoi diagram and geodesic Denaulay triangulation (Figure 2), since in $\mathcal{M}$ there may be several geodesics between any two points and any number (including

zero) of empty geodesic disks whose boundaries pass through any three points. In this paper, we prove that a duality between geodesic Voronoi diagram and geodesic Denaulay triangulation does exist in manifold $\mathcal{M}$ when the given point set P includes all cone points in $\mathcal{M}$ and satisfies two assumptions from Section 3. This duality is unique, since the Delaunay tessellation of P in $\mathcal{M}$ was proved to be unique [2].

3 Geodesic Voronoi Diagram and Its Duality

The traditional discrete Laplace operator [4] depends on the original triangulation T of $\mathcal{M}$. By observing its drawbacks of possibly negative weights and non-intrinsic property, the key idea in [2] is to use a Delaunay triangulation of the same cone point set V of $\mathcal{M}$ for defining an intrinsic discrete Laplace-Beltrami operator. In this paper, we study the geodesic Voronoi diagram of the cone point set V and its duality for a geodesic Delaunay triangulation of V in $\mathcal{M}$.

Let $P = \{p_1, p_2, \cdots, p_m\}$ be a set of points in $\mathcal{M}$ and its geodesic Voronoi diagram consists of Voronoi cells $\mathcal{GVD}(P) = \{\mathcal{VC}(p_1), \mathcal{VC}(p_2), \cdots, \mathcal{VC}(p_m)\}$. The boundary of each Voronoi cell $\mathcal{VC}(p_i)$ consists of Voronoi edges separated at Voronoi vertices. Each Voronoi edge in $\mathcal{GVD}(P)$ is incident to two Voronoi cells and each Voronoi vertex in $\mathcal{GVD}(P)$ is incident to at least three Voronoi edges.

Edelsbrunner and Shah [5] proposed a closed ball property, and Dyer et al. [3] showed that if a geodesic Voronoi diagram satisfies this closed ball property, a dual intrinsic Delaunay triangulation exists. The closed ball property has three conditions:

1. each Voronoi cell is homeomorphic to a planar disk,
2. the intersection of any two Voronoi cells is either empty or a single Voronoi edge or a single Voronoi vertex,
3. the intersection of any three Voronoi cells is either empty or a single Voronoi vertex.

A region $\Omega \subset \mathcal{M}$ is strong convex if given any two points $p_1, p_2 \in \Omega$, there is a unique minimum geodesic connecting p_1 and p_2 whose interior is contained in Ω and there is no other geodesic connecting p_1 and p_2 in Ω. Dyer et al. (Theorem 1 in [3]) proved that if for every Voronoi cell $\mathcal{VC}(v_i)$, there exists a strong convex region Ω_i such that $\mathcal{VC}(v_i) \subset \Omega_i$, then a dual intrinsic Delaunay triangulation exists. However, as shown below, the proof of Theorem 1 in [3] for condition 2 in the closed ball property is incorrect.

3.1 Assumptions

A *pseudo-bisector* of a point p in $\mathcal{M}$ is a set Q of points satisfying that there are two or more different geodesic paths of the same length from p to a point $q \in Q$. An example is illustrated in Figure 3(a). Pseudo-bisectors can be readily obtained by utilizing the geodesic distance structure in [12] and practical implementations were proposed in [8, 9, 10].

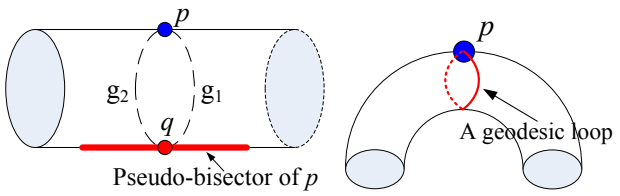

(a) Pseudo-bisector (b) Geodesic loop

Figure 3: (a) A pseudo-bisector (shown in red) of a point p on a cylinder model, in which a point q have two different geodesics (g_1 and g_2) of the same length to the source p. (b) A geodesic loop passes through p in a multi-connected Voronoi cell $\mathcal{VC}(p)$.

Assumption 1 *For no point $p_i \in P$ does the Voronoi cell $\mathcal{VC}(p_i)$ contain a pseudo-bisector of p_i.*

Given an arbitrary simplicial 2-manifold $\mathcal{M} = \{V, E, T\}$, we use Algorithm 1 to construct a sampling point set P that satisfies Assumption 1.

Algorithm 1 Sampling a simplicial 2-manifold mesh to satisfy Assumption 1

1: Let $P = V$.
2: Construct $\mathcal{GVD}(P)$ using the algorithm in [9].
3: Check Assumption 1.
4: If there is a Voronoi cell $\mathcal{VC}(p_i)$ that contains a pseudo-bisector $PB(p_i)$ of p_i, perform Step 6.
5: Else Stop
6: Choose a point q in $PB(p_i)$ and add q into P. Locally update $\mathcal{GVD}(P)$ and go to Step 3.

We show without proof that there are at most $O(m)$ points added into P by Algorithm 1, where m is the number of cone points. Accordingly Algorithm 1 terminates in finite time.

Assumption 2 *Any pair of distinct vertices, $p_i \neq p_j \in P$, whose Voronoi cells intersect at a Voronoi edge, has a unique geodesic between p_i and p_j.*

The number of geodesic paths between two points p_i and p_j can be obtained by utilizing the geodesic distance structure in [12] and we use practical implementations in [8, 9, 10]. Given an arbitrary simplicial 2-manifold $\mathcal{M} = \{V, E, T\}$, we use Algorithm 2 to construct a sampling point set P that satisfies Assumption 2.

We show without proof that if the degree of each vertex in the mesh is bounded by a constant C, there are at

Algorithm 2 Sampling a simplicial 2-manifold mesh to satisfy Assumption 2

1: Let $P = V$.
2: Construct $\mathcal{GVD}(P)$ using the algorithm in [9].
3: Check Assumption 2. If there are Voronoi cells $\mathcal{VC}(p_i)$ and $\mathcal{VC}(p_j)$ sharing some Voronoi edges and there are more than one geodesic between p_i and p_j, perform Step 4. Otherwise stop.
4: Let $g_1, g_2, \cdots, g_m$, $m > 1$, be the set of geodesics between p_i and p_j. For $1 < k \leq m$, let q_k be the midpoint in g_k and add q_k into P, i.e., $P = q_k \cup P$. Locally update $\mathcal{GVD}(P)$ and go to Step 3.

most $O(m)$ points added into P by Algorithm 2, where m is the number of cone points. Accordingly Algorithm 2 terminates in finite time.

3.2 Closed ball property

Lemma 1 *If Assumptions 1 and 2 hold, each Voronoi cell in $\mathcal{GVD}(P)$ is homeomorphic to a planar disk.*

Proof. If there is a Voronoi cell $\mathcal{VC}(p_i)$ in $\mathcal{GVD}(P)$ is not homeomorphic to a planar disk, then its boundary consists of at least two closed curves and we say the Voronoi cell $\mathcal{VC}(p_i)$ is multi-connected (Figure 3(b)). Then there must exist a geodesic loop going through p_i inside $\mathcal{VC}(p_i)$. Accordingly, a pseudo-bisector of p_i must be contained in $\mathcal{VC}(p_i)$; a contradiction to Assumption 1. □

Lemma 2 *If there are two geodesics between two points in $\mathcal{M}$, then there must be at least one cone point inside the region enclosed by these two geodesics.*

Proof. The discrete geodesic structure revealed in [12] shows that a geodesic goes through a set of triangles and cone points (Figure 1). If two geodesics passing through the same set of triangles and cone points, these two geodesics must be the same since after unfolding the passed triangles, there is only one straight line segment between two points in the unfolded plane. That completes the proof. □

Lemma 3 *If Assumptions 1 and 2 hold, for any Voronoi cell $\mathcal{VC}(p_i)$ in $\mathcal{GVD}(P)$ and for any point q in the boundary $\partial\mathcal{VC}(p_i)$ of $\mathcal{VC}(p_i)$, the geodesic between p_i and q is inside $\mathcal{VC}(p_i)$.*

Proof. As illustrated in Figure 4(a), let q be a point in $\partial\mathcal{VC}(p_i)$ whose geodesic g_{p_iq} to p_i goes outside of $\mathcal{VC}(p_i)$ and enters into $\mathcal{VC}(p_j)$. Let a be a point in the geodesic g_{p_iq} that is also inside $\mathcal{VC}(p_j)$. Then we have $d_g(p_i, q) = d_g(p_j, q) = d_g(p_i, a) + d_g(a, q)$. Since $d_g(p_i, a) > d_g(p_j, a)$, we have $d_g(p_j, q) > d_g(p_j, a) + d_g(a, q)$, a contradiction to the triangle inequality of the geodesic metric in $\mathcal{M}$. □

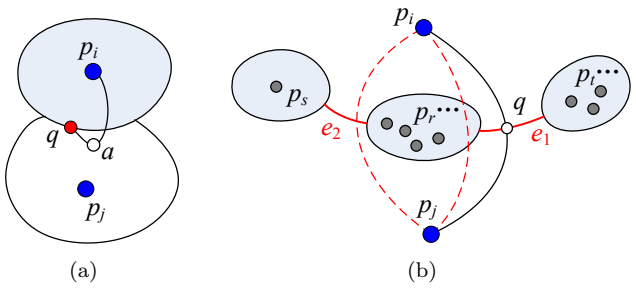

Figure 4: (a) A point q in a Voronoi edge shared by two Voronoi cells $\mathcal{VC}(p_i)$ and $\mathcal{VC}(p_j)$. (b) There are two geodesics (shown in dashed red lines) between p_i and p_j, if two cells $\mathcal{VC}(p_i)$ and $\mathcal{VC}(p_j)$ share two separated Voronoi edges e_1 and e_2 (shown in solid red line).

Lemma 4 *If Assumptions 1 and 2 hold, the intersection of any two Voronoi cells in $\mathcal{GVD}(P)$ is either empty or a single Voronoi edge or a single Voronoi vertex.*

Proof. If this lemma does not hold, then there exist two Voronoi cells $\mathcal{VC}(p_i)$ and $\mathcal{VC}(p_j)$ whose intersection consists of at least two separated Voronoi edges e_1 and e_2. As shown in Figure 4(b), let q be a point in e_1. Then the geodesics g_{p_iq} and g_{p_jq} form a path l between p_i and p_j. Note that l pass through a set Θ of triangles that can be unfolded into a plane. In all the paths passing through the same set Θ of triangles connecting p_i and p_j, there must be a geodesic in Θ. Note that this geodesic may not go through the interior of e_1 as shown in Figure 4(b). Similarly, there is another geodesic connecting p_i and p_j corresponding to e_2. The two geodesics corresponding to e_1 and e_2 cannot be the same one by Lemma 2 since e_1 and e_2 is separated by the Voronoi cells of at least one cone point. Thus there are two distinct geodesics between p_i and p_j, a contradiction to Assumption 2. □

Note that in [3] the condition 2 of closed ball property is proved incorrectly by only considering the case that the shared bisector of $\mathcal{VC}(p_i)$ and $\mathcal{VC}(p_j)$ is separated by a region that is the Voronoi cell of a single point (Figure 5). Our proof is based on the most general case that the separated regions can consist of several Voronoi cells (Figure 4(b)). A real example of this general case is shown in Figure 6.

Lemma 5 *If Assumptions 1 and 2 hold, the intersection of any three Voronoi cells in $\mathcal{GVD}(P)$ is either empty or a single Voronoi vertex.*

Proof. In this paper we consider a simplicial 2-manifold mesh without boundary. Then there are at least four mesh vertices and the sampling point set P has at least four samples. It was shown in [3] that if there are at least four samples and the conditions 1 and

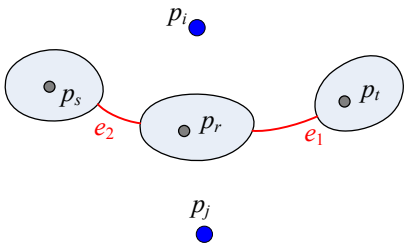

Figure 5: The proof in [3] only considers the case that the bisector (shown in red) is separated by a region that is the Voronoi cell of a single point.

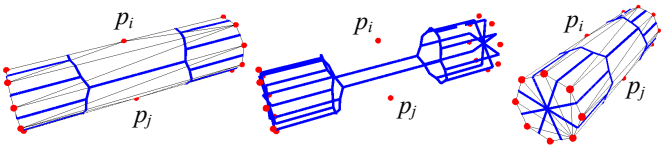

Figure 6: A general case that is not considered in the proof in [3]: the Voronoi cells $\mathcal{VC}(p_i)$ and $\mathcal{VC}(p_j)$ share two separated Voronoi edges, which are separated by regions consisting of eight Voronoi cells. Left: the Voronoi diagram (shown in blue) of all mesh vertices (shown in red) in a cylinder mesh. Middle: the Voronoi diagram without surface rendering. Right: Another view of the Voronoi diagram in the mesh surface.

2 in closed ball property are satisfied, the condition 3 is also satisfied. □

By Lemmas 1, 4, 5 and the closed ball property, we have

Theorem 6 *If the sampling point set P ($V \subset P$) satisfies the Assumptions 1 and 2, the geodesic Voronoi diagram $\mathcal{GVD}(P)$ has a dual intrinsic Delaunay triangulation.*

Given a set P of m sampling points and a simplicial surface of genus g with n vertices, it was shown in [9, 11] that the geodesic Voronoi diagram $\mathcal{GVD}(P)$ can be constructed in $O(n^2 \log n)$ time and the number of Voronoi vertices and Voronoi edges in $\mathcal{GVD}(P)$ is $O(m+g)$. Since in our case the sampling point set P include all cone points, we have $m \geq n$ and the number of Voronoi vertices and Voronoi edges in $\mathcal{GVD}(P)$ is $O(m)$. Given the structure of geodesic Voronoi diagram $\mathcal{GVD}(P)$, we assume the computation of the unique geodesic between two source points in P whose Voronoi cells share a Voronoi edge takes $O(1)$ time. Then we have

Theorem 7 *Given a set P of m sampling points on a simplicial surface S that satisfies the Assumptions 1 and 2, the intrinsic Delaunay triangulation of P on S can be constructed in $O(m^2 \log m)$ time and take $O(m)$ space.*

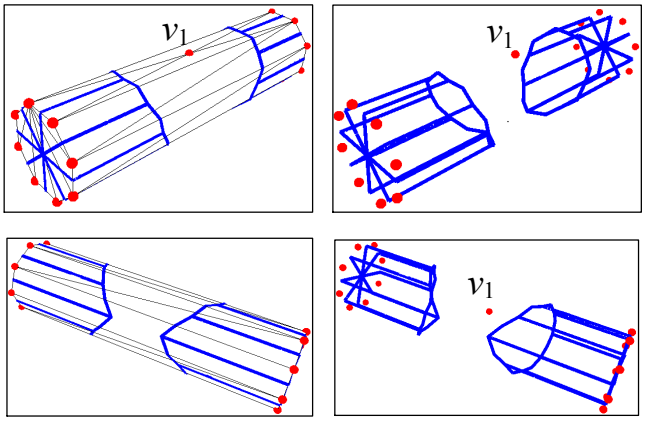

Figure 7: A cylinder mesh model: the Voronoi cell of v_1 in the geodesic Voronoi diagram (shown in blue) is multi-connected and contains a pseudo-bisector. Top row: the front view with and without surface rendering. Bottom row: the back view with and without surface rendering.

4 Practical Examples and Experiments

In the presented experiment, we illustrate the process of how to obtain a sampling point set P on a simplicial surface S that satisfies the two assumptions. Then we construct geodesic Voronoi diagram and the dual intrinsic Delaunay triangulation of P on S.

A cylinder mesh model is shown in Figure 7. We first run the Algorithm 1 to obtain a sampling point set P satisfying Assumption 1. The process of Algorithm 1 is illustrated in Figures 7 and 8. In more details, first we let $P = V$ and the geodesic Voronoi diagram is shown in Figure 7. For the Voronoi cell $VC(v_1)$ that is multi-connected, there is a pseudo-bisector in $VC(v_1)$ and a new sample point p_1 is added into P. The resulting updated geodesic Voronoi diagram is shown in Figure 8.

Then we run Algorithm 2 to update the sampling point set P further satisfying Assumption 2. In the geodesic Voronoi diagram shown in Figure 8, there are two geodesics between v_1 and p_1 (Figure 9(a)). A new sample point p_2 is added into P (Figure 9b) and the geodesic Voronoi diagram is updated (Figure 9(c)). Finally the dual intrinsic Delaunay triangulation is constructed (Figure 9(d)).

Geodesic Voronoi diagrams and the dual intrinsic Delaunay triangulations on some more realistic models are shown in Figure 10. In these models, there are thousands to tens of thousands of triangles and the running time of building geodesic Voronoi diagram and dual intrinsic Delaunay triangulations is within 10 seconds on a PC (Intel(R) Core(TM) I7C2600 CPU 3.40GHz, 8GB memory) running Windows 7.

Given an original mesh $\mathcal{M} = (V, E, T)$ without

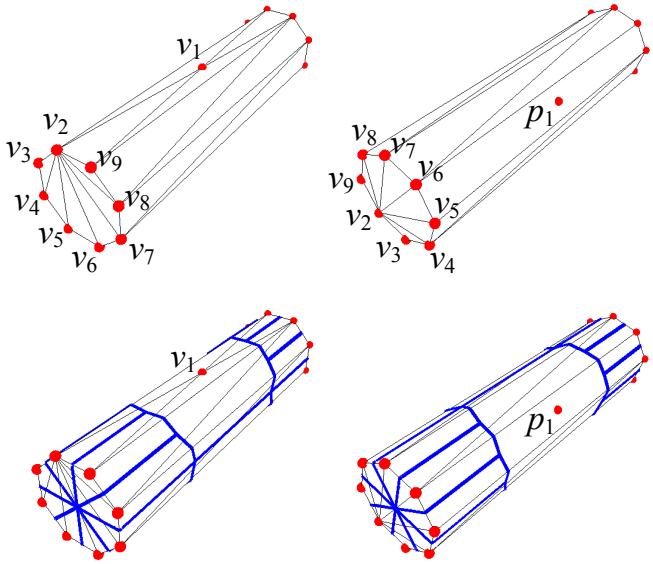

Figure 8: A point p_1 lying the pseudo-bisector of v_1 in $VC(v_1)$ (shown in Figure 7) is added and inserted into P. Top row: the cylinder mesh with a new added point p_1. Bottom row: the updated Voronoi diagram.

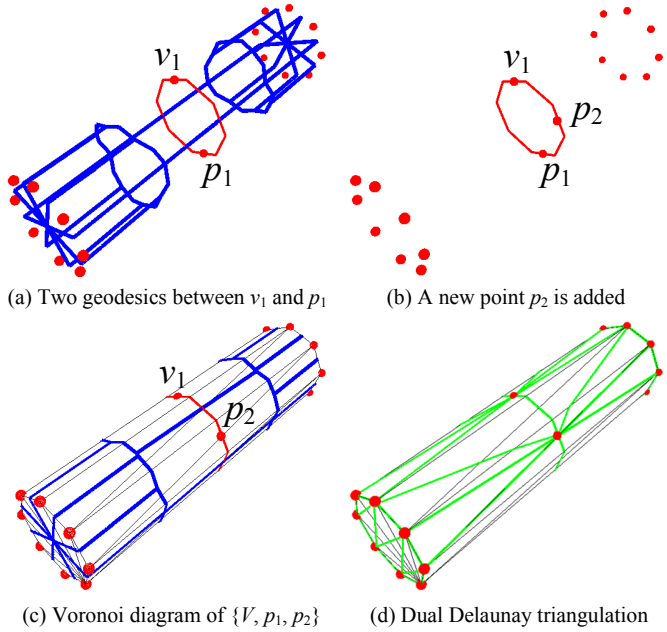

(a) Two geodesics between v_1 and p_1 (b) A new point p_2 is added

(c) Voronoi diagram of $\{V, p_1, p_2\}$ (d) Dual Delaunay triangulation

Figure 9: The process of Algorithm 2 in the model shown in Figure 8. The sampling points are shown in red dots, the geodesics are shown in red lines, the Voronoi diagram is shown in blue and the dual intrinsic Delaunay triangulation is shown in green.

boundary, the Laplace operator is defined as

$$\Delta f(v_i) = \sum_{v_j \in V:(v_i,v_j)\in E} w_{ij}(f(v_i) - f(v_j)) \qquad (1)$$

where $f : \mathcal{M} \to \mathbb{R}$ is a piecewise linear function on $\mathcal{M}$,

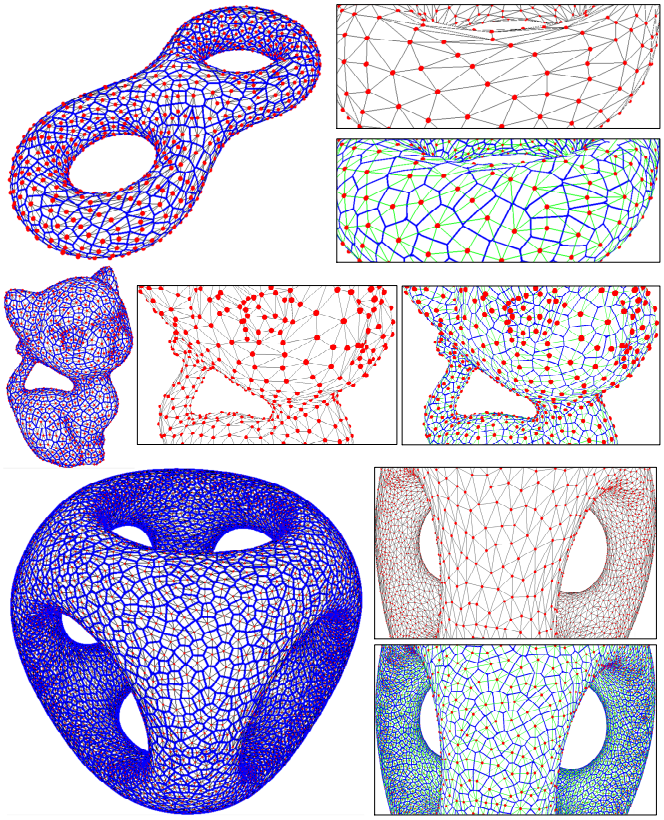

Figure 10: Geodesic Voronoi diagrams and dual intrinsic Delaunay triangulations on three realistic models. Red dots: mesh vertices; Black lines: original mesh; Blue lines: geodesic Voronoi diagram; Green lines: Dual intrinsic Delaunay triangulation.

and the edge weights are

$$w_{ij} = \frac{1}{2}(\cot \alpha_{ij} + \cot \alpha_{ji}) \qquad (2)$$

α_{ij} and α_{ji} are the angles opposite to edge (v_i, v_j) in two incident triangles. The Laplace operator is the gradient of the Dirichlet energy

$$E(f) = \frac{1}{2} \sum_{(v_i,v_j)\in E} w_{ij}(f(v_i) - f(v_j))^2, \qquad (3)$$

which resembles the continuous version $E(f) = \frac{1}{2}\int_S \|\nabla f\|^2$ on a Riemannian manifold $\mathcal{S}$. If we replace the connectivity information in Equations (1), (2) and (3) by (V, E', T') in the Delaunay triangulation of $\mathcal{M}$, the Laplace operator becomes the discrete Laplace-Beltrami operator [2]. If f is the identity map on $\mathbb{R}^3$ restricted to $\mathcal{M}$, then the discrete mean curvature vector $\mathcal{H}(v_i)$ at $v_i \in V$ is $\mathcal{H}(v_i) = \Delta f(v)$ and the discrete mean curvature vector density is $H(v_i) = \frac{\Delta f(v_i)}{Area(\mathcal{VC}(v_i))}$, where $Area(\mathcal{VC}(v_i))$ is the area of Voronoi cell $\mathcal{VC}(v_i)$.

We use the Laplace operator and the discrete Laplace-Beltrami operator to compute the discrete mean cur-

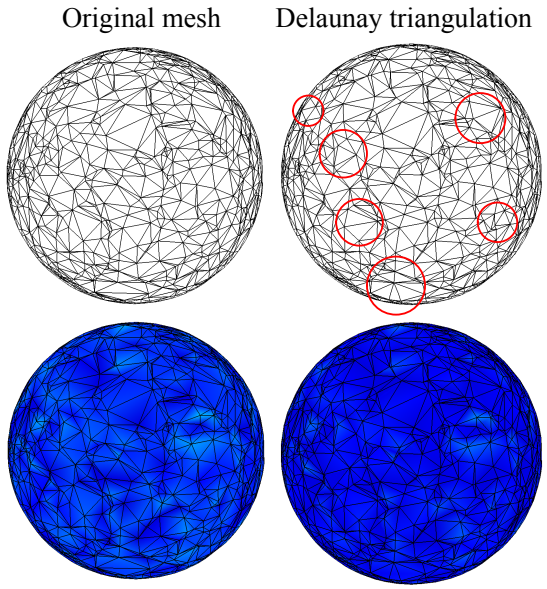

Figure 11: The discrete mean curvature (the second row, shown with a color mapping) computed on (left) the original irregular mesh and (right) the Delaunay triangulation. Some significant differences between the original mesh and Delaunay triangulation are circled.

vatures on original irregular meshes discretized from sphere, ellipsoid, paraboloid, hyperboloid, and their intrinsic Delauany triangulations, respectively. Since the ground truth of the mean curvatures on these parametric surfaces is known, we can compare the accuracy of these two computations. Here we only report the results on the irregular spherical mesh. The detailed numerical results should be presented elsewhere. An original irregular spherical mesh and its Delauany triangulation are shown in Figure 11 (the first row). The discrete mean curvatures computed based on these two triangulations are shown in Figure 11 (the second row). The numerical result shows that (1) the average error in the Laplace operator on the original irregular mesh is 3.89% and the average error in the discrete Laplace-Beltrami operator on the Delauany triangulation is 1.77%, (2) the maximum error in the Laplace operator on the original irregular mesh is 22.07% and the average error in the discrete Laplace-Beltrami operator on the Delauany triangulation is 13.26%. These results show that compared to extrinsic operators, the intrinsic Laplace-Beltrami operator based on the intrinsic Delauany triangulation has better numerical properties.

5 Conclusion

Recently a new intrinsic discrete Laplace-Beltrami operator was proposed in [2], which can find a wide range of applications in mesh smoothing, editing, parameterization and animation, etc. The computation of the intrinsic discrete Laplace-Beltrami operator depends on an intrinsic Delaunay triangulation on simplicial surfaces. Previously the only known method to compute the intrinsic Delaunay triangulation is the edge flipping algorithms [6, 7], which did not have provable theoretical complexity bounds. In this paper, we prove that when a sampling point set in a simplicial surface satisfies two assumptions, the duality between geodesic Voronoi diagram and the intrinsic Delaunay triangulation exists. Thus the intrinsic Delaunay triangulation can be obtained from a duality of the geodesic Voronoi diagram, whose time complexity is $O(m^2 \log m)$ and space complexity is $O(m)$, where m is the number of vertices in the intrinsic Delaunay triangulation.

Acknowledgement

The authors thank the reviewers very much for their insightful comments and detailed suggestions that improve this paper. This work was supported by the Natural Science Foundation of China (61322206, 61272228), the National High Technology Research and Development Program of China (2012AA011801) and Tsinghua University Initiative Scientific Research Program (20131089252).

References

[1] L.V. Ahlfors and L. Sario. *Riemann Surfaces*. Princiton University Press, 1960.

[2] A.I. Bobenko and B.A. Springborn. A discrete Laplace-Beltrami operator for simplicial surfaces. *Discrete & Computational Geometry*, vol. 38, no. 4, pp. 740-756, 2007.

[3] R. Dyer, H. Zhang and T. Moller. Surface sampling and the intrinsic Voronoi diagram. *Proceedings of the Symposium on Geometry Processing*, pp.1393-1402, 2008.

[4] G. Dziuk. Finite elements for the Beltrami operator on arbitrary surfaces. In S. Hildebrandt and R. Leis eds., *Partial Differential Equations and Calculus of Variations*. Lecture Notes in Mathematics, vol. 1357, pp. 142–155, Springer, 1988.

[5] H. Edelsbrunner and N.R. Shah. Triangulating topological spaces. *International Journal of Computational Geometry and Applications*, Vol. 7, No. 4, pp. 365-378, 1997.

[6] M. Fisher, B. Springborn, A.I. Bobenko and P. Schroder. An algorithm for the construction of intrinsic delaunay triangulations with applications to digital geometry processing. *ACM SIGGRAPH 2006 Courses*, pp. 69-74, 2006.

[7] C. Indermitte, T.M. Liebling, M. Troyanov and H. Clemencon. Voronoi diagrams on piecewise flat surfaces and an application to biological growth. *Theoretical Computer Science*, Vol. 263, No. 1-2, pp. 263–274, 2001

[8] Y.J. Liu, Q.Y. Zhou and S.M. Hu. Handling degenerate cases in exact geodesic computation on triangle meshes. *The Visual Computer*, vol. 23, no. 9-11, pp. 661-668, 2007.

[9] Y.J. Liu, Z.Q. Chen and K. Tang. Construction of iso-contours, bisectors and voronoi diagrams on triangulated surfaces. *IEEE Transactions on Pattern Analysis and Machine Intelligence*, vol. 33, no. 8, pp. 1502–1517, 2011.

[10] Y.J. Liu. Exact geodesic metric in 2-manifold triangle meshes using edge-based data structures. *Computer-Aided Design*, vol. 45, no. 3, pp. 695-704, 2013.

[11] Y.J. Liu and K. Tang. The Complexity of geodesic Voronoi diagrams on triangulated 2-manifold surfaces. *Information Processing Letters*, vol. 113, no. 4, pp. 132-136, 2013.

[12] J. Mitchell, D. Mount, C. Papadimitriou. The discrete geodesic problem. *SIAM Journal on Computing*, vol. 16, no. 4, pp. 647-668, 1987.

[13] A. Okabe, B. Boots, K. Sugihara and S.N. Chiu. *Spatial Tesselations: Concepts and Applications of Voronoi Diagram*. Sec. Ed., Chichester: Wiley, 2000.

[14] U. Pinkall and K. Polthier. Computing discrete minimal surfaces and their conjugates. *Experimental Mathematics*, vol. 2, no. 1, pp. 15-36, 1993.

[15] S. Rosenberg. *The Laplacian on a Riemannian Manifold: An Introduction to Analysis on Manifolds*. Cambridge University Press, 1997.